Efficient, selective sodium and lithium removal by Faradaic deionization using symmetric sodium titanium vanadium phosphate intercalation electrodes

Aniruddh Shrivastava,[a,‡] *Vu Q. Do,*[a, ‡] *and Kyle C. Smith*[a,b,c,d]*

[a] Department of Mechanical Science and Engineering, University of Illinois at Urbana-Champaign, Urbana, IL, USA

[b] Department of Materials Science and Engineering, University of Illinois at Urbana-Champaign, Urbana, IL, USA

[c] Computational Science and Engineering Program, University of Illinois at Urbana-Champaign, Urbana, IL, USA

[d] Beckman Institute for Advanced Science and Technology, University of Illinois at Urbana-Champaign, Urbana, IL, USA

[‡]These authors contributed equally

*Corresponding author's email: kcsmith@illinois.edu

ABSTRACT

NASICON (sodium superionic conductor) materials are promising host compounds for the reversible capture of Na^+ ions, finding prior application in batteries as solid-state electrolytes and cathodes/anodes. Given their affinity for Na^+ ions, these materials can be used in Faradaic deionization (FDI) for the selective removal of sodium over other competing ions. Here, we investigate the selective removal of sodium over other alkali and alkaline earth metal cations from aqueous electrolytes when using a NASICON based mixed Ti-V phase as an intercalation electrode, namely sodium titanium vanadium phosphate (NTVP). Galvanostatic cycling experiments in three-electrode cells with Na^+, K^+, Mg^{2+}, Ca^{2+} and Li^+ reveal that only Na^+ and Li^+ can intercalate into the NTVP crystal structure, while other cations show capacitive response, leading to material-intrinsic selectivity factors of 56 for Na^+ over K^+, Mg^{2+} and Ca^{2+}. Further, electrochemical titration experiments together with modeling show that an intercalation mechanism with limited miscibility gap for Na^+ in NTVP mitigates the state-of-charge gradients to which phase-separating intercalation electrodes are prone when operated under electrolyte flow. NTVP electrodes are then incorporated into a FDI cell with automated fluid recirculation to demonstrate up to 94% removal of sodium in streams with competing alkali/alkaline earth cations with ten-fold higher concentration, showing process selectivity factors of 3-6 for Na^+ over cations other than Li^+. Decreasing current density can improve selectivity up to 25% and reduce energy consumption by as much as ~50%, depending on the competing ion. The results also indicate the utility of NTVP for selective lithium recovery.

KEYWORDS: electrochemical deionization, selectivity, intercalation, NASICON, phase equilibria, desalination, lithium recovery

1. INTRODUCTION

Present water scarcity[1] and its potential exacerbation by climate change[2] motivate the desalination of salt-rich water resources to increase freshwater access. While human-potable water is a significant need, agriculture accounts for the most water use globally by humans among all sectors,[3] presenting a unique opportunity to selectively remove micronutrient sodium that competes for uptake into crops together with potassium, magnesium, and calcium macronutrients.[4,5] For example, in 2011 the US had 5.4 million acres of saline cropland with another 76.2 million being at risk.[6] Recent analysis estimates an annual economic loss of ~$1000/acre due to lower crop yield,[7] motivating the desalination of groundwater and brackish water for agricultural purposes.[8] While using desalinated water for irrigation has improved yield up to 30%,[9] remineralization is required to supply macronutrients using conventional desalination processes.[10] Despite pressure and thermally driven processes comprising the majority of global desalination capacity,[11] they lack ion selectivity. Therefore, energy-efficient selective removal of sodium is a potential alternative to desalination with remineralization. In addition to desalination, certain industrial separation processes such as purification of potassium-based salts[12,13] require selective removal of Na^+ over other alkali and alkaline earth cations.

Capacitive deionization using electric double layers (EDLs) in activated carbon electrodes has been proposed for selective sodium removal,[5] but EDLs are only weakly selective based on hydrated ionic radius and charge number.[14,15] Alternatively, redox-active cation intercalation materials have been investigated in selective Faradaic deionization (FDI) processes. Nickel hexacyanoferrate (NiHCF) has been used to demonstrate selective removal of Na^+ over divalent ions such as Mg^{2+} and Ca^{2+}.[16] However, NiHCF shows 10:1 preference for K^+ over Na^+,[17] and hence exhibits the reverse order of selectivity to that which is desired (Na^+ over K^+). Further, the potential

degradation of NiHCF by Ni^{2+} substitution with Mg^{2+} or Ca^{2+} poses a challenge to the long-term life of such a system.[18] Using sodium titanium phosphate (NTP) and sodium manganese oxide (NMO), selective removal of Na^+ over other ions in diluate feed streams has shown preferential capture of Na^+,[19] but the standard reduction potential for Na^+ intercalation into NTP is extremely low (-0.8 V vs Ag/AgCl), leading to hydrogen evolution, poor coulombic efficiency (CE), and high energy consumption.[19]

Despite these limitations the broader class of sodium superionic conductor (NASICON) materials to which NTP belongs show high charge capacity and fast solid-state sodium diffusion, as supported by their use in solid-state electrolytes,[20–22] lithium-ion batteries,[23] and sodium-ion batteries as cathodes[24–27] and anodes.[28–31] These properties also make NASICON materials attractive candidates for selective removal of Na^+ in FDI. Among NASICONs, sodium vanadium phosphate ($Na_3V_2(PO_4)_3$; NVP) shows high specific capacity (~118 mAh/g) and density (3.25 g/cm^3),[24,32–34] theoretically producing three-fold higher solid-state cation-storage concentration (14 mol-Na^+/L) than commonly used Prussian blue analogues (5 mol-Na^+/L).[35] Further, the standard reduction potential of the V^{3+}/V^{4+} couple for the intercalation of Na^+ in NVP at +0.3 V vs Ag/AgCl is highly suitable for applications in aqueous electrolytes.[36,37] Despite earlier reports using NVP in a dual-ion type FDI process,[38] NVP/C suffers from dissolution in water during oxidation of V^{3+} to V^{4+},[39] motivating its partial substitution with titanium to form $Na_2TiV(PO_4)_3$ (NTVP) to enable stable operation of the $V^{3+/4+}$ redox couple in water.[39]

Despite their promise based on battery-like experiments, the performance of cation intercalation materials in practical FDI cells additionally depends on the arrangement of flow channels and flow conditions. Flowing feed water *through porous electrodes* – as motivated by modeling[40–42] – has been shown experimentally to increase salt removal,[35] salt removal rate,[43] and thermodynamic

energy efficiency[35,44] compared to feed-water flow either *by or behind electrodes*. Even so, the streamwise gradients in ion concentration that are inherent to deionization processes have been linked to streamwise gradients in the state-of-charge of intercalation material,[42,43] where phase-separating NASICON has exhibited pronounced gradients[40] relative to solid-solution intercalation materials (e.g., NiHCF[41,42]). While feed-water recirculation has been used to minimize such state-of-charge gradients,[35,42,45] the relative merits of phase-separating and solid-solution mechanisms has yet to be quantified among NASICONs, as we presently do.

In this article, we investigate the selectivity of NTVP for Na^+ over K^+, Mg^{2+}, Ca^{2+}, NH_4^+, and Li^+ using a combination of electrochemical characterization and Faradaic deionization experiments. Insights into cation-storage mechanisms are first obtained through three-electrode flooded cells, including solid-state phase equilibria and the distinction between cation intercalation into NTVP versus cation adsorption into EDLs on its surface. NTVP electrodes are then incorporated into an FDI cell with automatic feed-water recirculation to demonstrate the selective removal of sodium from various feed streams with up to ten times higher concentration of competing ions. The effect of current density on the selectivity and energy consumption is analyzed, and the major advantages and limitations are discussed.

2. EXPERIMENTAL METHODS

2.1. SYNTHESIS AND CHARACTERIZATION OF NTVP/C PARTICLES

A sol-gel procedure was adopted from various sources in literature[36,39,46,47] and optimized to synthesize $Na_2TiV(PO_4)_3$ powders coated with carbon (NTVP/C). Briefly, citric acid monohydrate (0.02 M) was used as a reduction and chelation agent and was mixed with ammonium metavanadate (0.02 M) and sodium dihydrogen phosphate (0.06 M) to form a 100 mL solution in deionized water. This solution was heated at 80°C on a hot plate and vigorously stirred till a dark

109 blue solution was obtained, indicating complete reduction of V^{5+} to V^{4+}. This solution was allowed
110 to cool to room temperature. In a separate dry beaker, glacial acetic acid (0.02M) and titanium
111 isopropoxide (0.02 M) were dissolved in pure ethanol to obtain a 100 mL solution. The second
112 solution was poured into the first solution under vigorous stirring, to obtain a whitish green turbid
113 dispersion. This mixture was heated at 80°C until the volume reached ~100 mL before being
114 transferred to a large petri dish and heated at the same temperature under vacuum to evaporate all
115 remaining solvents. A bluish green xerogel was obtained, which was ground into fine powders
116 using a mortar-pestle. These powders were transferred to porcelain crucibles and heated under N_2
117 flow (2-3 L/min) in a tube furnace at 350°C for 5 h, followed by heating at 800°C for 12 hours,
118 with a ramp rate of 3°C/min for all temperature ramps. Black crystalline powders were obtained
119 after cooling the samples to room temperature, indicating the formation of carbon-coated
120 $Na_2TiV(PO_4)_3$ powder. Sodium vanadium phosphate was also synthesized using the same
121 procedure as above, without the addition of titanium isopropoxide by adjusting concentrations
122 accordingly for vanadium precursor. Powder X-ray diffraction was performed using a Siemens
123 Bruker D8 instrument. The relative composition of transition metal elements in the as synthesized
124 powders was measured using energy dispersive X-Ray fluorescence (EDXRF, Shimadzu EDX-
125 7000).

126 2.2 FABRICATION OF ELECTRODES

127 Porous electrodes were made from NTVP active particles, Ketjenblack (KB) conductive
128 additive, and polyvinylidene fluoride (PVDF) binder with the weight ratio of 80:5:15. The mixture
129 of NTVP particles with KB was ground in a vortex mill with 5 mm steel balls (Ultra Turra-X,
130 IKA) at 6000 rpm for 10 to 15 minutes to obtain a fine, homogeneous powder. PVDF was dissolved
131 in N-methyl-2-pyrrolidone (NMP, Sigma Aldrich) to form a 16.2 wt.% solution. The NTVP and

KB powder were further added to this solution and mixed in a planetary mixer (Thinky, ARE-310) for 30 minutes. The resulting slurry was cast onto graphite foil (Ceramaterials) current collectors that have a thickness of ~120μm using a doctor blade and film applicator (Elcometer 4340). These electrodes were immersed in deionized water for wet phase inversion and were subsequently dried in a fume hood, followed by heating in an oven at 70°C for 2-3 hours to give ~150μm thickness after solidification. Electrodes were punched into 1 cm^2 circular disks for flooded cell experiments and were cut into 1.7x1.5 cm^2 pieces for FDI experiments. The electrodes prepared had a high mass loading of 8-11 mg/cm^2.

2.3 ELECTROCHEMICAL CHARACTERIZATION AND FARADAIC DEIONIZATION EXPERIMENTS

All electrochemical experiments were performed using a Biologic VMP-3 potentiostat. Flooded cell experiments used NTVP working electrodes, Ag/AgCl reference electrodes (0.199V vs. SHE, Pine Research), and a graphite rod (Gamry) as a counter electrode. In preparation for FDI experiments one electrode was charged completely at a C-rate of C/10 to remove Na^+ ions while the other was completely discharged, both in a flooded cell. These electrodes were assembled and operated in a custom-built FDI flow cell using galvanostatic cycling. The design, operation, and flow-calibration of this cell is described in our previous work.[35,43] Briefly, the cell had two NTVP electrodes separated by a Neosepta AMX anion exchange membrane (Astom Corp) sandwiched between two graphite current collectors (McMaster-Carr). Here, feed water was forced to flow through porous electrodes via a 3D-printed fluid-distribution unit. Diluate and concentrate effluent were generated simultaneously during the experiment and were recirculated back to the respective electrodes as influent. At the end of each half-cycle when the electrodes were fully (de)intercalated, influent streams were swapped between the two electrodes so as to cause continuous desalination

155 water in the diluate reservoir. This was performed by using four servos to pinch a branched rubber
156 tubing system to ensure influent from one reservoir flows through only one electrode. A Masterflex
157 peristaltic pump maintained a single constant flow rate in both diluate and concentrate streams
158 throughout desalination experiments. The effluents in all experiments were checked with pH paper
159 and found no change in pH. The concentration of individual cations within influent and effluent
160 water was measured using a 930 Compact IC system from Metrohm with a Metrosep C4 – 150/4.0
161 cation column calibrated against standard samples whose ion concentrations ranged between 1 –
162 100ppm (Supporting Information, Section S1). Specific energy consumption (SEC) was estimated
163 for each experiment by assuming that the fraction of electrical energy invested for Na removal was
164 proportional to its fraction of total cationic charge removed from solution, as determined from *ex*
165 *situ* IC.
166

167 ## 3. RESULTS AND DISCUSSION

168 We first present the structural and electrochemical characterization of NTVP/C powders, after
169 which we present the results of cycling NTVP electrodes in an FDI flow cell. Intercalation of Na^+
170 into the NTVP crystal is studied using equilibrium potential data from intermittent titration
171 experiments and regular solution modeling to reveal no apparent miscibility gap at equilibrium for
172 intercalation into NTVP, as opposed to high miscibility gaps leading to two-phase intercalation
173 observed in NVP and NTP. Theory is then used to predict the impact of miscibility gap on the
174 uniformity of electrode state-of-charge under flowing conditions. Galvanostatic cycling
175 experiments in a flooded cell with other electrolytes containing K^+, Li^+, Mg^{2+}, and Ca^{2+} were
176 performed to determine the intrinsic selectivity of NTVP for Na^+ over other cations. Finally, FDI
177 experiments using feed water with different cation concentrations and compositions were

178 performed to characterize process selectivity and energy consumption, and highly selective capture
179 of Na^+ over other cations is observed.

180 3.1 ELECTROCHEMICAL CHARACTERIZATION OF NTVP/C ELECTRODES

181 Sol-gel synthesis of carbon-coated NTVP was shown to produce a crystal structure in the *R-3c*
182 space group with lattice parameters (a=8.6 Å and c=21.8 Å) in agreement with literature (Fig.
183 S1).[31] Energy dispersive X-ray fluorescence also revealed the molar ratio of Ti to V as 0.97 in
184 close agreement with the nominal formula of NTVP. Galvanostatic cycling of NTVP and NVP
185 prepared using similar syntheses was performed to assess material stability. NTVP is shown to
186 stabilize after the first 10 cycles at 1C with high coulombic efficiency (Fig. 1(a,b)). Further, even
187 after all experiments presented in this article our NTVP electrodes retained a similar capacity level
188 in a three-electrode flooded cell even after approximately 150 prior cycles. In contrast, 80% of
189 NVP's capacity is lost after one charge step when NVP is cycled in 500 mM NaCl (Fig. S2) with
190 V^{4+} dissolution evidenced by the yellowing of its electrolyte. Though the specific capacity
191 produced by NTVP (45 mAh/g) is less than half that of NVP (110 mAh/g), it corresponds to a
192 solid-state cation-storage concentration of 5.4 mol-Na^+/L, which is similar to that of NiHCF[35] that
193 is commonly used in FDI.

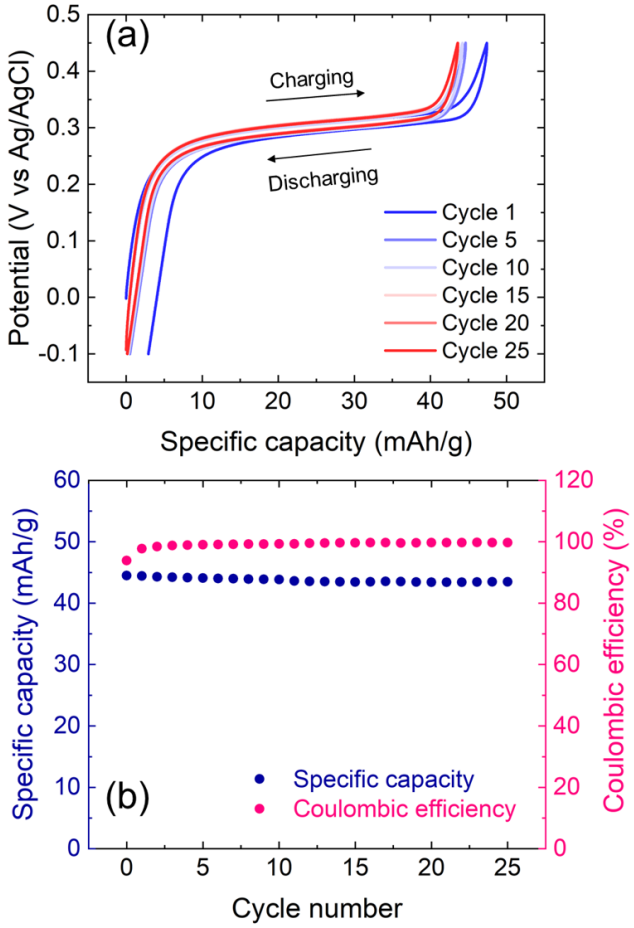

Figure 1. Charge/discharge profile of (a) sodium titanium vanadium phosphate (NTVP) in 0.5 M NaCl at 1C. (b) Variation of specific capacity and coulombic efficiency of NTVP with cycle number in 0.5 M NaCl.

To understand the interaction of Na^+ ions with the NTVP crystal, equilibrium potential curves in 500 mM NaCl were measured using galvanostatic intermittent titration (GITT). Here, small current pulses (C/40) were applied for 5 mins to inject 2.5% of the total charge capacity during each pulse, followed by relaxation for 40 mins after each pulse. Fig. 2(a) shows the equilibrium potential ϕ_{eq} versus the degree of intercalation x obtained from GITT. In contrast with NVP and NTP that possess non-zero miscibility gaps (92%[48] and 71%,[49] respectively) over which two-phase coexistence occurs during intercalation, the binary NASICON material NTVP shows a continuous

decrease of potential with increasing x, similar to NiHCF.[50] The low miscibility gap of NTVP is evident from the differential capacity obtained from GITT experiments, where 80% of its charge capacity is achieved within a 60mV potential range (Fig. 2(b)). This range is much wider than that shown for materials with first-order phase transformations.[51]

To characterize the impact of material composition on the interaction energy Ω between the reduced and oxidized endmembers of NTVP we fitted a regular solution model to the potential variations measured from GITT. Here, the equilibrium potential ϕ_{eq} for Na^+ intercalation is expressed as (Supporting Information, Section S2):

$$\phi_{eq} = \phi_{eq}^0 + kT\ln[(1-x)/x]/e + \Omega(2x-1)/e \quad (1)$$

where ϕ_{eq}^0, k, T, and e are the material's standard reduction potential for Na^+ intercalation, the Boltzmann constant, temperature, and the elementary charge, respectively. Here, the degree of intercalation x varies from 0 to 1, and the interaction energy Ω quantifies the degree of attractive/repulsive energies between endmember phases of the NTVP host.[52,53] Fig. 2(b) shows that NVP and NTP possess interaction energies greater than $2kT$ ($2.50kT$ and $3.45kT$, respectively) causing phase separation during Na^+ intercalation. In contrast, NTVP produces an approximate interaction energy of $0.57kT$, minimizing the occurrence of phase separation at equilibrium. Therefore, the partial substitution of vanadium in NVP with titanium as done here significantly reduces the interaction parameter between endmember phases. However, the interaction energy for NTVP is still slightly higher than in Prussian blue analogues that exhibit potentials similar to ideal solutions.[50,54] While the sloping potential profile and small interaction parameter observed for the equilibrium intercalation into NTVP resembles that of a solid-solution mechanism, we note that previous observations by synchrotron X-ray diffraction during non-aqueous intercalation utilizing both the Ti and V redox couples have shown some degree of phase

separation.[46] Therefore, *in situ* synchrotron X-ray diffraction and/or solid-state NMR are required to directly probe phase behavior during intercalation into NTVP in aqueous electrolytes, where intercalated or crystal H_2O may also play a role in stabilizing solid-solution cation intercalation.[55]

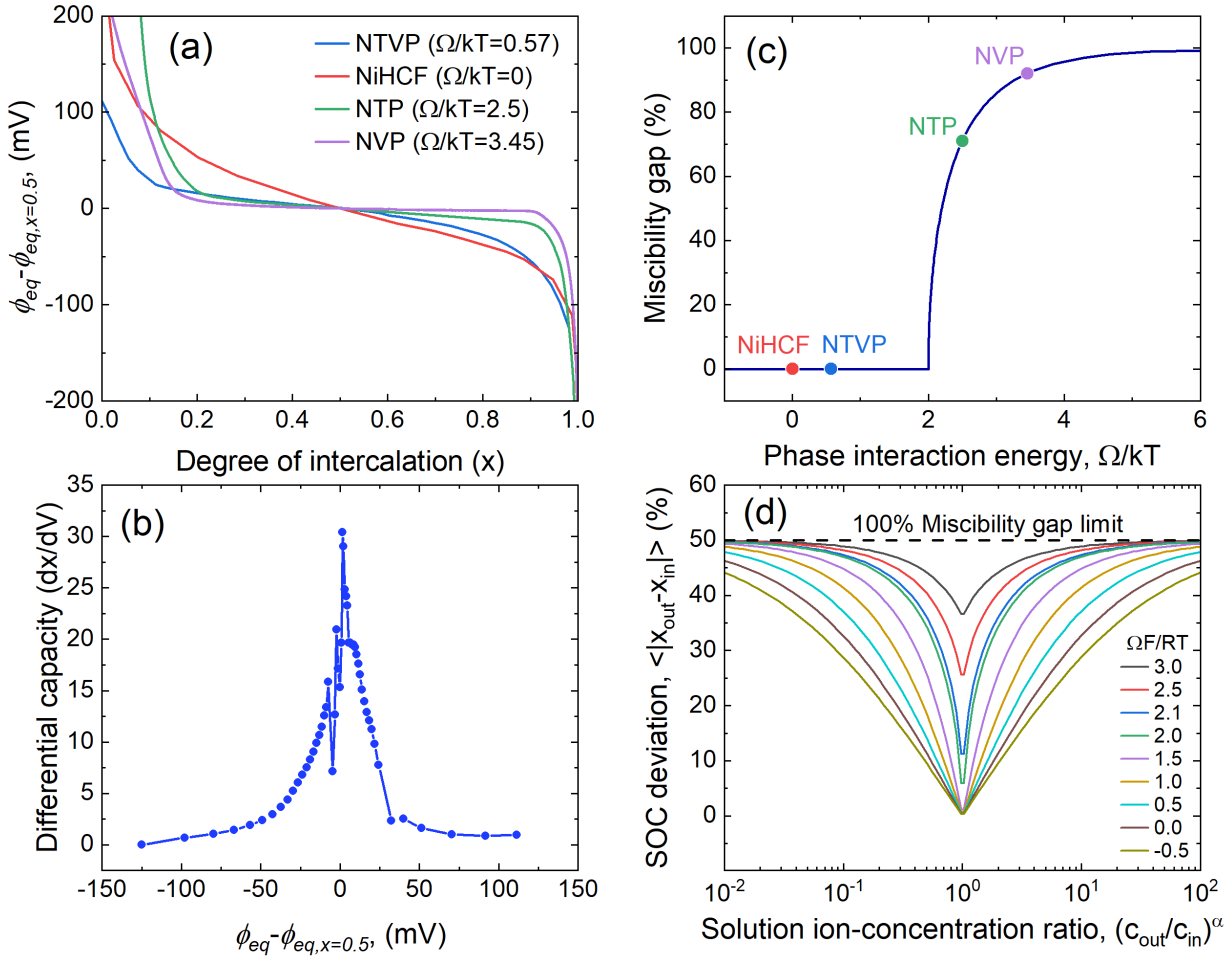

Figure 2. (a) Equilibrium potential curve obtained from a room-temperature GITT experiment on NTVP ($\phi_{eq,0.5}$ = 0.291V vs. Ag/AgCl) fitted to a regular solution model (this work), along with curves estimated for NTP ($\phi_{eq,0.5}$ = -0.751V vs. Ag/AgCl)[40,49] and NVP ($\phi_{eq,0.5}$ = 0.321V vs. Ag/AgCl) (this work) from galvanostatic cycling and for NiHCF ($\phi_{eq,0.5}$ = 0.355 V vs. Ag/AgCl)[41,56] from potentiostatic intermittent titration. (b) Differential capacitance of NTVP estimated from GITT data. (c) Miscibility gap versus fitted interaction energy at ~300K and (d)

modeled average state-of-charge deviation $\langle|x_{out} - x_{in}|\rangle$ across an electrode to produce an effluent cation concentration c_{out} from feedwater with cation concentration c_{in}.

To investigate the impact of these material-specific interactions on FDI performance *a priori*, we constructed a theoretical model that links intercalation reaction-rate distributions to the streamwise gradients of cation concentration in solution that are inherent to flow-cell operation. Inspired by our previous work, we assume facile intercalation kinetics, facile solid-state transport, and negligible streamwise current density[42] to show that the difference in the equilibrium potential between the ends of an electrode depends on the ratio of cation concentrations in solution at its ends (see Supporting Information, Section S2):

$$\phi_{eq}(x_{out}) - \phi_{eq}(x_{in}) = -kT\ln[c_{out}/c_{in}]^{\alpha} \tag{2}$$

Here, the exponent α takes on different values depending on whether the cation of interest is part of a binary electrolyte ($\alpha = 2(1 - t_{+})$, where t_{+} is the transference number of intercalating cations in solution) or a minority ion in a supporting electrolyte as for selective separations ($\alpha = 1$). By solving this equation numerically for the outlet degree-of-intercalation x_{out} for certain x_{in}, c_{out}, c_{in}, and Ω, we calculated an average measure of the state-of-charge deviation across the electrode $\langle|x_{out} - x_{in}|\rangle$ as follows:

$$\langle|x_{out} - x_{in}|\rangle = \int_{0}^{1} |x_{out} - x_{in}|\, dx_{in} \tag{3}$$

As shown in Fig. 2(c), this state-of-charge deviation in general is lowest for materials having phase interaction energies commensurate with low miscibility gap and/or solid-solution intercalation, while for two-phase materials increased miscibility gap results in maximal state-of-charge non-uniformity. Hence, the decreased interaction energy within NTVP relative to NVP

and NTP shows promise for efficient and resilient cycling in FDI systems due to its ability to minimize phase separation and state-of-charge gradients.

Building on these results we characterized the intercalation of different alkali and alkaline-earth cations into the NTVP crystal using galvanostatic cycling, as shown in Fig. 3(a) for cycling experiments separately using aqueous electrolytes with 500 mM of LiCl, NaCl, KCl, $MgCl_2$, and $CaCl_2$. Several trends are observed. Similar to Na^+ intercalation into NTVP, Li^+ shows stable cycling in NTVP with a low miscibility gap. However, Li^+ intercalation produces a specific capacity of approximately 30 mAh/g, which is 33% lower than the capacity for Na^+ intercalation. This lower capacity for Li^+ intercalation indicates that there are likely one-third of the sites in the NTVP crystal that are inaccessible to Li^+ ions, despite being accessible to Na^+ for intercalation. Further, the standard reduction potential for Li^+ intercalation is approximately 70 mV lower than that of Na^+ (0.24 V for Li^+ vs 0.31 V for Na^+, vs Ag/AgCl). Assuming equivalent site occupation statistics for Na^+ and Li^+ in the NTVP crystal and assuming thermodynamic equilibrium, this difference in potential $\Delta\phi$ implies a selectivity ratio β at room temperature of approximately 16:1 for Na^+ to Li^+ using the appropriate Boltzmann factor: $\beta = \exp(-\Delta\phi/kT)$. In contrast with Li^+ and Na^+, all other alkali and alkaline-earth cations show capacitive response that produces ~10X smaller specific capacity (5-6 mAh/g), suggesting that the cycling of electrolytes containing such cations results in EDL charge-storage and not intercalation into the NTVP crystal. Therefore, these results indicate a selectivity sequence of $Na^+ > Li^+ >>> K^+ \approx Mg^{2+} \approx Ca^{2+}$ for electrosorption by NTVP electrodes.

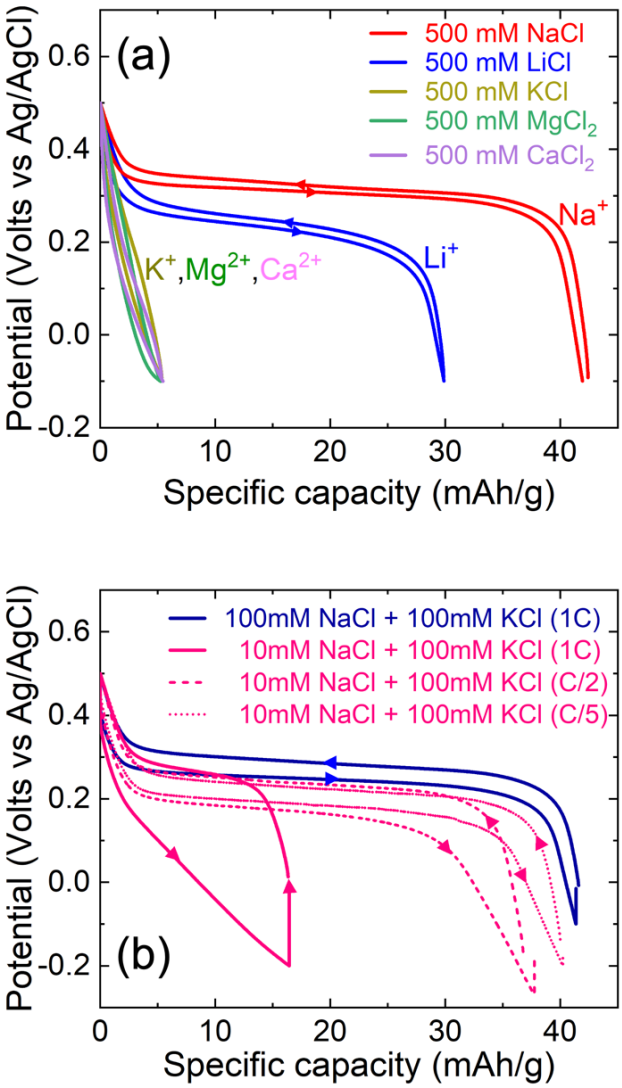

Figure 3. Galvanostatic cycling in a three-electrode flooded cell with (a) electrolytes comprised of 0.5 M NaCl, LiCl, KCl, $MgCl_2$ and $CaCl_2$ at a C-rate of 1C and (b) mixed solutions of KCl and NaCl operated at different C-rates.

Fig. 3(b) shows the results of flooded-cell galvanostatic cycling in electrolytes with 100 mM KCl + 100 mM NaCl, and 100 mM KCl + 10 mM NaCl at C-rates of 1C and C/2. The variation of potential with capacity at C/2 rate indicates an intercalation process with a low miscibility gap, which can be attributed to the insertion of Na^+ ions. Cycling at 1C in 100 mM KCl + 10 mM NaCl shows less than 50% capacity than with 100 mM KCl + 100 mM NaCl. Further, in the case with

288 only 10 mM NaCl, discharge and charge potential variations are highly asymmetric. These results
289 can be attributed to the low ratio of Na^+ to K^+ in the electrolyte (1:10). During discharge with low
290 Na^+ concentration in the electrolyte (10 mM), potential response is limited by the electrolyte-phase
291 diffusion of Na^+ ions. Therefore, a semi-linear potential profile is obtained. However, during
292 charging, since Na^+ ions travel from within NTVP into the electrolyte, the potential response as a
293 function of the degree of intercalation x follows the usual intercalation profile. When the applied
294 current is lowered to C/5, solid-state diffusion of Na^+ ions within the NTVP porous electrode
295 becomes rate-limiting during both discharge and charge, as evidenced by the potential response.
296 Based on the specific capacity results obtained by cycling in electrolytes containing both
297 monovalent and divalent ions as shown for Figs. 3(a) and 3(b), an intrinsic selectivity factor of the
298 electrodes can be calculated for Na^+ relative to other cations. For the case of 100 mM KCl + 10
299 mM NaCl, almost all the capacity at C/5 rate can be attributed to the intercalation of Na^+. From
300 Fig. 3(a), a maximum of 6 mAh/g of can be absorbed from KCl solutions, which can be subtracted
301 from the total specific capacity calculated in the mixed ion solution to obtain the minimum amount
302 of Na^+ intercalated. The lack of a redox plateau suggests that such capacity for cycling in KCl
303 electrolyte is purely a result of adsorption into EDLs at the surfaces of NTVP particles, conducting
304 additives, and current collectors. Building on this postulate the selectivity of Na^+ over K^+ is infinite
305 for intercalation into the NTVP crystal. However, in the aqueous electrolytes of interest to us for
306 water treatment EDLs readily form, resulting either in the adsorption of K^+ or the expulsion of Cl^-
307 . Hence, a finite selectivity ratio will be achieved in practice. The capacitive charge-storage
308 mechanism for ions other than Na^+ and Li^+ also suggests a way of tuning the selectivity ratio of
309 Na^+ and K^+ by modifying the surface area of the NTVP electrodes, including by using different
310 conductive additives or by physical modification NTVP/C particles. From the present

311 galvanostatic cycling experiments, we estimate a selectivity ratio $\beta_{Na/K}$ by using measured
312 capacities while assuming that co-ion expulsion of Cl^- is negligible in EDLs:

313 $$\beta_{Na/K} = \frac{[Na^+_{captured}]}{[K^+_{captured}]} \times \frac{[K^+_{electrolyte}]}{[Na^+_{electrolyte}]} = \frac{(40-6)mAh/g}{6\,mAh/g} \times \frac{100\,mM}{10\,mM} = 56.67 \quad (4)$$

314 Therefore, porous electrodes of NTVP/C are at least 56 times more selective for capturing Na^+
315 over K^+. Similar estimates are obtained for Mg^{2+} and Ca^{2+} based on the above calculation. Note
316 that this selectivity factor is for the active material combined with capacitive contributions from
317 the carbon domains in the electrodes. In our subsequent results using NTVP electrodes in a
318 continuous-flow FDI cell we show that *process selectivity* for Na^+ – determined based on the
319 concentrations of ions in effluent streams – is smaller than the *material selectivity* determined from
320 flooded-cell experiments, due to the additional physicochemical mechanisms that are at play in
321 flow cells.

322 3.2 SELECTIVITY AND ENERGY CONSUMPTION OF A SYMMETRIC NTVP/C FDI
323 FLOW CELL

324 Encouraged by its high selectivity for Na^+ over other cations obtained from flooded-cell
325 characterization, we tested NTVP/C electrodes in the continuous-flow FDI cell developed in our
326 previous work.[35,43] Feed streams with varying ratios of Na^+ with one other competing ion, including
327 K^+, Mg^{2+}, Ca^{2+}, NH_4^+ and Li^+, were pumped through the cell to obtain two effluent streams
328 respectively containing diluted and concentrated Na^+. A constant flow rate of 1 mL/min was used
329 in all experiments. Ion composition of the diluate and concentrate reservoirs was measured using
330 ion chromatography. The composition of feed streams and the applied current used in each
331 experiment are listed in Table 1, and the results are presented in Fig. 4. When there is an abundance
332 of Na^+ and K^+ (Expt. 1) in equimolar ratio, the electrodes prefer to capture sodium, resulting in a
333 separation factor for the whole process of 15.25 (Fig. 4(a) and 4(b)). When the amount of sodium

334 in the feed stream is 10 times less than potassium (Expts. 2 & 3), the NTVP electrodes were still
335 able to capture more than 90% of sodium. Decreasing the applied current density from 0.5 mA/cm^2
336 (1.4C) to 0.25 mA/cm^2 (0.7C) led to a slight increase in sodium removal, while correspondingly
337 decreasing potassium removal, consistent with the results from flooded cell experiments.
338
339 **Table 1:** Feed stream concentrations and current density used in the experiments performed with
340 the symmetric FDI cells and NTVP/C electrodes for selective removal of Na^+.

Experiment number	Initial cation concentrations in feed stream (x mM Na^+ + y mM A^+) ($A=K^+$, Mg^{2+}, Ca^{2+}, Li^+, NH_4^+)	Current density (mA/cm^2)
1	100 Na^+ + 100 K^+	0.5
2	10 Na^+ + 100 K^+	0.5
3	10 Na^+ + 100 K^+	0.25
4	10 Na^+ + 100Mg^{2+}	0.5
5	10 Na^+ + 100Mg^{2+}	0.25
6	10 Na^+ + 100Ca^{2+}	0.5
7	50 Na^+ + 50 NH_4^+	0.5
8	20 Na^+ + 20 Li^+	0.5

341

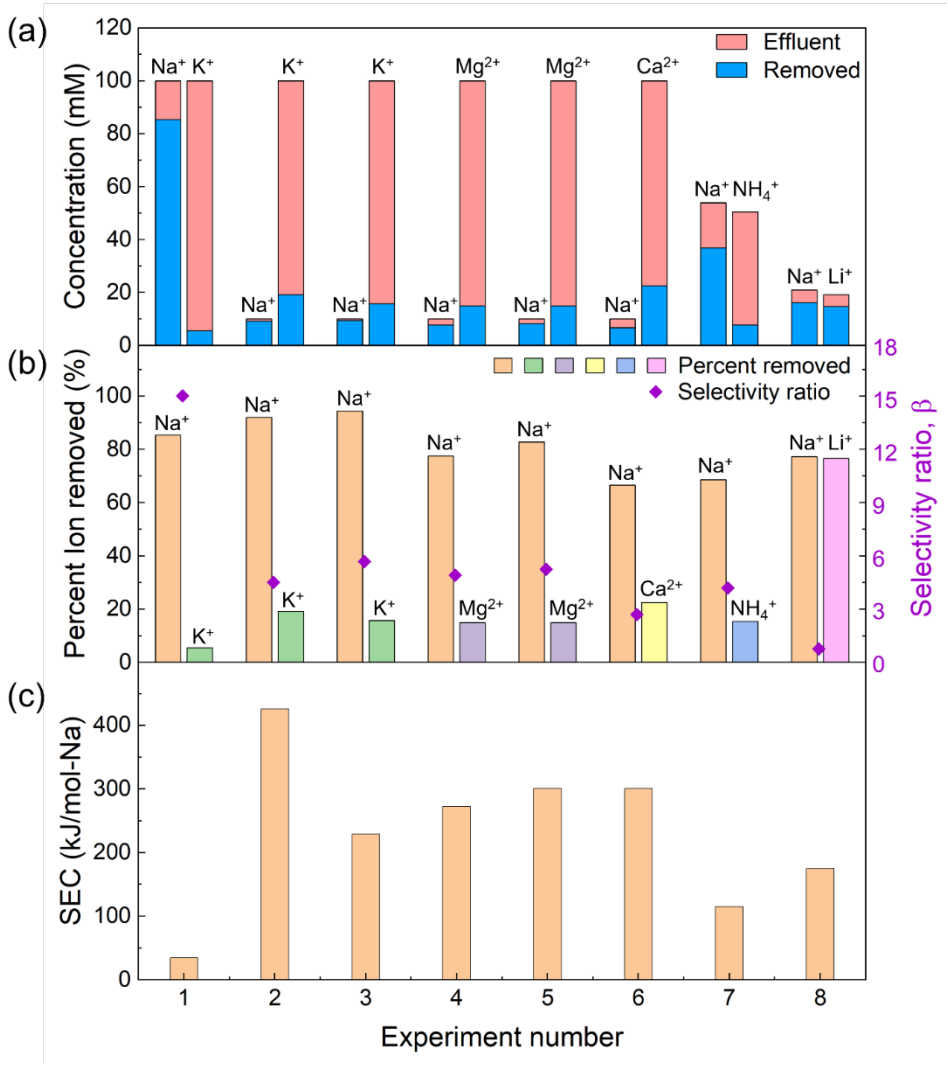

342

343 **Figure 4.** (a) Concentration of individual ions in the diluate stream with corresponding amount of

344 ion removal, (b) percent removal of ions and selectivity ratio, and (c) specific energy consumption

345 (SEC) for each mole of sodium being removed in each experiment listed in Table 1. SEC for Li

346 removal in the experiment using a 1:1 mixture of NaCl and LiCl is identical to that for Na removal.

347 Similarly, in feed streams with 1:10 of Na^+ to Mg^{2+}, 80% removal of Na^+ is obtained and with

348 1:10 of Na^+ to Ca^{2+} a removal of Na^+ close to 65% is obtained (Fig. 4a). In all experiments apart

349 from those using Li^+, selectivity ratios of 4 to 5 were obtained (Fig. 4b). The percent sodium

350 removal in the experiments with Mg^{2+}, Ca^{2+}, and NH_4^+ as the competing ion were slightly lower

than K^+, likely due to residual ions from previous experiments still adsorbed on electrode surfaces. It is worth mentioning that even though the theoretical selectivity of Na^+ over Li^+ was estimated as 16:1 based on measured intercalation potentials, we find that NTVP electrodes intercalate both cations to a similar degree when operating in an FDI cell to produce a separation factor of $\beta_{Na/Li} \approx 1$ (Figs. 4(a) and 4(b)). This result shows for the first time the promise of NTVP for Li^+ extraction applications.

Next, we attempt to understand the effects of feed-stream concentration and current densities on the selectivity and energy consumption of Na^+ removal. We focus on selectivity experiments with Na^+/K^+ and with Na^+/Mg^{2+} ions to highlight our insights, as shown in Figs. 4b,c. The variation of capacity with cycle number and voltage polarization curves for other experiments are included in the Supplementary Information (Figs. S3). At a 1:10 ratio of Na^+ to K^+, greater than 90% Na^+ is removed at current densities of both 0.25 mA/cm^2 and 0.5 mA/cm^2, and slightly higher Na^+ removal was achieved at lower current density, resulting in a 24% increase in selectivity factor from 4.8 to 5.97. Further, energy consumption nearly halves (Fig. 4c) due to a significant reduction in voltage polarization, as evidenced from the variation of cell voltage with specific capacity (Figs. 5a and 5b). Moreover, at 0.5 mA/cm^2 potential varies linearly with capacity (Fig. 5a) in an apparent pseudo-capacitive manner, as opposed to 0.25 mA/cm^2 where the saturation of intercalation sites is evident from sharp changes in potential at terminal capacity (Fig. 5b). The competition from K^+ ions to reach active-material surfaces compared to Na^+ seems to be significantly higher at greater current densities, likely due to the faster diffusion of K^+ in aqueous electrolytes than Na^+, along with its ten-fold higher concentration in the feed stream. Compared to flooded-cell cycling with NaCl, there is significantly higher voltage polarization in the FDI process, likely due to ohmic resistance caused by the AEM and electronic/ionic resistance within the porous electrodes, in

addition to Donnan polarization caused by the concentration difference across the AEM. However, in experiments with Mg^{2+} as the competing ion (Expts. 4 & 5) halving the current density does not lead to a significant change in selectivity (only 5% increase of β in Fig. 4b), and in fact such decreased current increases the energy consumption for selective Na^{+} removal by ~10% (Fig. 4c). Therefore, the effect of ion-specific selectivity factors and energy consumption requires deeper study. In principle, the presence of excess competing ions on electrode surfaces could crowd the surface of NTVP and limit the amount of sodium that can be intercalated. This phenomenon has been examined in the case of NTP and NMO materials, although in solutions with an order of magnitude lower ionic strength.[19]

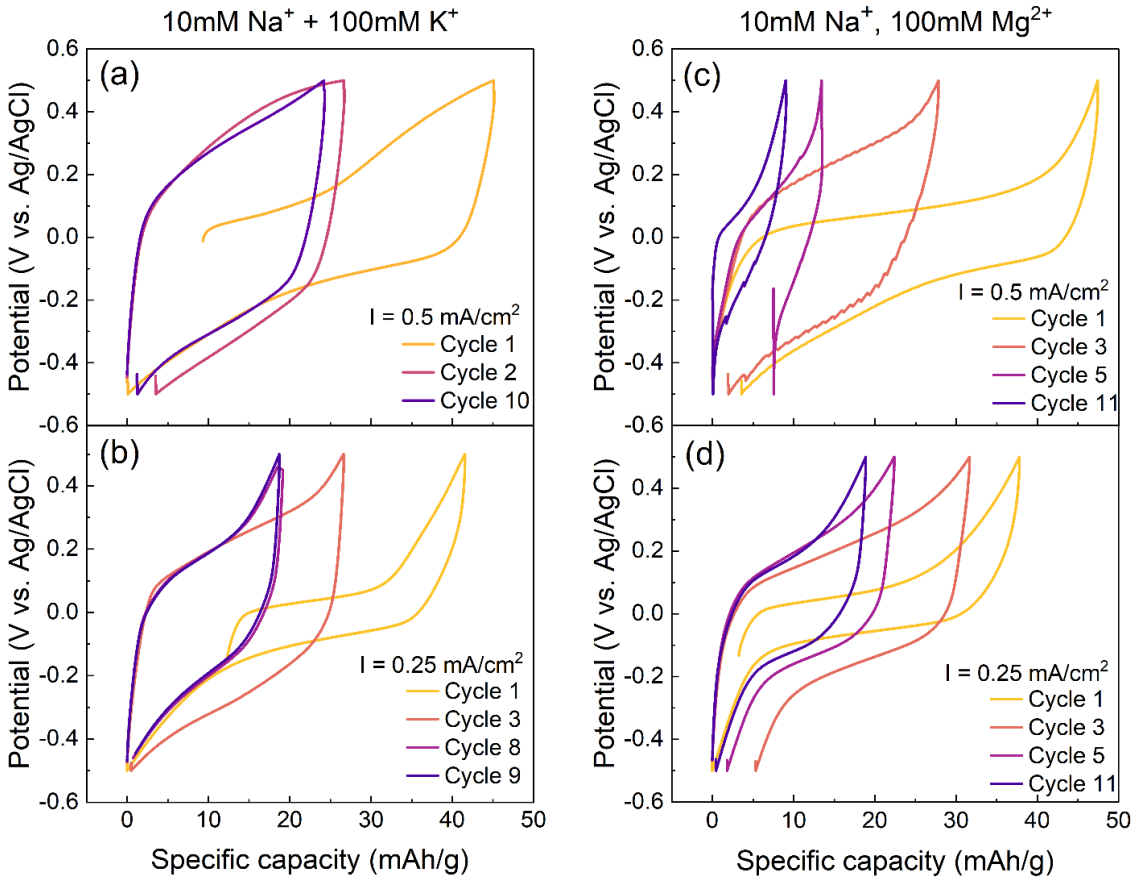

Figure 5. Variation of potential with specific capacity for different charge/discharge cycles for Expts. 2 and 3 (a)-(b) and Expts. 4 and 5 (c)-(d) from Table 1 with feed-stream concentration and applied current density as shown.

Unlike the case with K^+ as a competing ion where pseudo-capacitive contributions dominate after the initial cycles at higher current density (Figs. 5a and 5b), potential variation with capacity in the case of electrolytes mixed with Mg^{2+} and Na^+ indicate solid-solution intercalation mechanisms at both 0.5 mA/cm^2 and 0.25 mA/cm^2 (Figs. 5c and 5d) for all cycles. This contrasting behavior likely indicates lesser crowding of NTVP surfaces when Na^+ ions compete with Mg^{2+} compared to K^+.

397 We further analyze the energy consumption for selective Na^+ removal obtained in these
398 experiments and compare to previous work. It is important to note however that we used automated
399 fluid control for continuous deionization for many charge/discharge cycles. Most existing works
400 in literature involve either manually moving the electrodes between fresh and concentrated
401 solutions, or manually swapping the diluate and concentrate streams after completion of every
402 charge or discharge cycle. Capacitive deionization with sulfonated electrodes has been used to
403 selectively remove sodium from brackish water for irrigation, which consumes 0.2 – 0.4kWh/m^3
404 for 4 – 6mM removal of Na^+, about 150 – 200 kJ/mol of salt removal, but the separation factor
405 was only 1.6.[57] A rocking-chair battery using NMO/KFeHCF electrodes was able to remove
406 sodium-ion impurities from KCl with 4.46 Wh/g-Na, which translates to 69 kJ/(mol-
407 Na).[13] Membrane technology has been shown through mathematical modeling to be capable of
408 maintaining sodium concentration below the threshold level of 20 mM in irrigation water for
409 tomatoes with an energy consumption of 0.7-2.5 kWh/m^3 for a 360 g/h sodium removal at 1.48
410 m^3/h volumetric flowrate to produce 252 – 900 kJ/mol sodium removed.[5] For the majority of
411 experiments presented here the present NTVP symmetric FDI cell consumed less than or equal to
412 300 kJ/mol sodium removed (Fig. 4c) when operating with ten-fold higher concentration of
413 competing alkali/alkaline earth cations than sodium, which is among the most efficient devices for
414 selective removal of sodium to our knowledge. Further, our results using 1:1 feed water mixtures
415 of NaCl and LiCl indicate that Li^+ removal occurs with similarly low SEC.

416 Further examination reveals that specific capacity decreases rapidly after 4 to 6 cycles and
417 remains approximately constant afterwards for the cases where NaCl is mixed with either KCl,
418 $MgCl_2$ or $CaCl_2$ at ten-fold higher concentrations (Figs. 6a- 6e). Our preceding results suggest that
419 most sodium is removed during a few early cycles and that the charge capacity obtained in later

cycles is mainly due to capacitive adsorption of competing ions, consistent with our results obtained from flooded-cell experiments (Fig. 3a). As a consequence, we posit that the energy consumed in later cycles is inconsequential to Na^+ removal and is therefore consumed unnecessarily. To quantify this effect we estimate the ratio of the cumulative charge transferred to NTVP by sodium intercalation Q_{acc} over a set of cycles, relative to the total charge of sodium removed Q_{Na} for the five experiments shown in Figs. 6a-6e. Q_{Na} was determined *ex situ* by ion chromatography on water effluent. Q_{acc} was calculated by subtracting the charge due to capacitive adsorption, as estimated by the minimum capacity obtained from all cycles of a given experiment, from the cumulative charge delivered via external circuit. As can be seen from Figs. 6a – 6e, Q_{acc} exceeds $0.95Q_{Na}$ after 4 – 7 cycles (the number of yellow columns in each experiment), meaning that 95% of the sodium removal is obtained in a few early cycles, in agreement with our prior reasoning. Hence, energy consumption is likely to be 30 to 50% lower if determined from those few cycles, as compared to after the 10 – 20 cycles tested here (Fig. 6f). In particular, the energy consumption at 0.5 mA/cm^2 and 0.25 mA/cm^2 in the presence of 100 mM KCl would be 297 kJ/mol-Na and 127kJ/mol-Na, respectively. Similarly for 100 mM $MgCl_2$ and 10 mM NaCl, the energy consumption will drop to 171 kJ/ mol-Na and 155 kJ/mol-Na for the respective current densities of 0.5 and 0.25 mA/cm^2. For the case when 100 mM $CaCl_2$ was the competing ion, the energy consumption will also reduce to 192 kJ/mol-Na. In addition, FDI *process selectivity* is likely to approach the values of NTVP material selectivity if the experiments were stopped after those few early cycles due to the decreases in competing ions removal by capacitive adsorption. We note here that the values of Q_{acc}/Q_{Na} of the last cycles in Figs. 6a – 6e are higher than one due to the assumption that CE is 100%. These points motivate further investigation to determine cycle-to-cycle variations of selectivity and energy consumption, to minimize energy input and to

443 maximize selectivity. In addition, reductions in energy consumption are likely achievable via
444 improved electrode fabrication to yield high mass loading, low binder content, and high electrical
445 conductivity.[35]

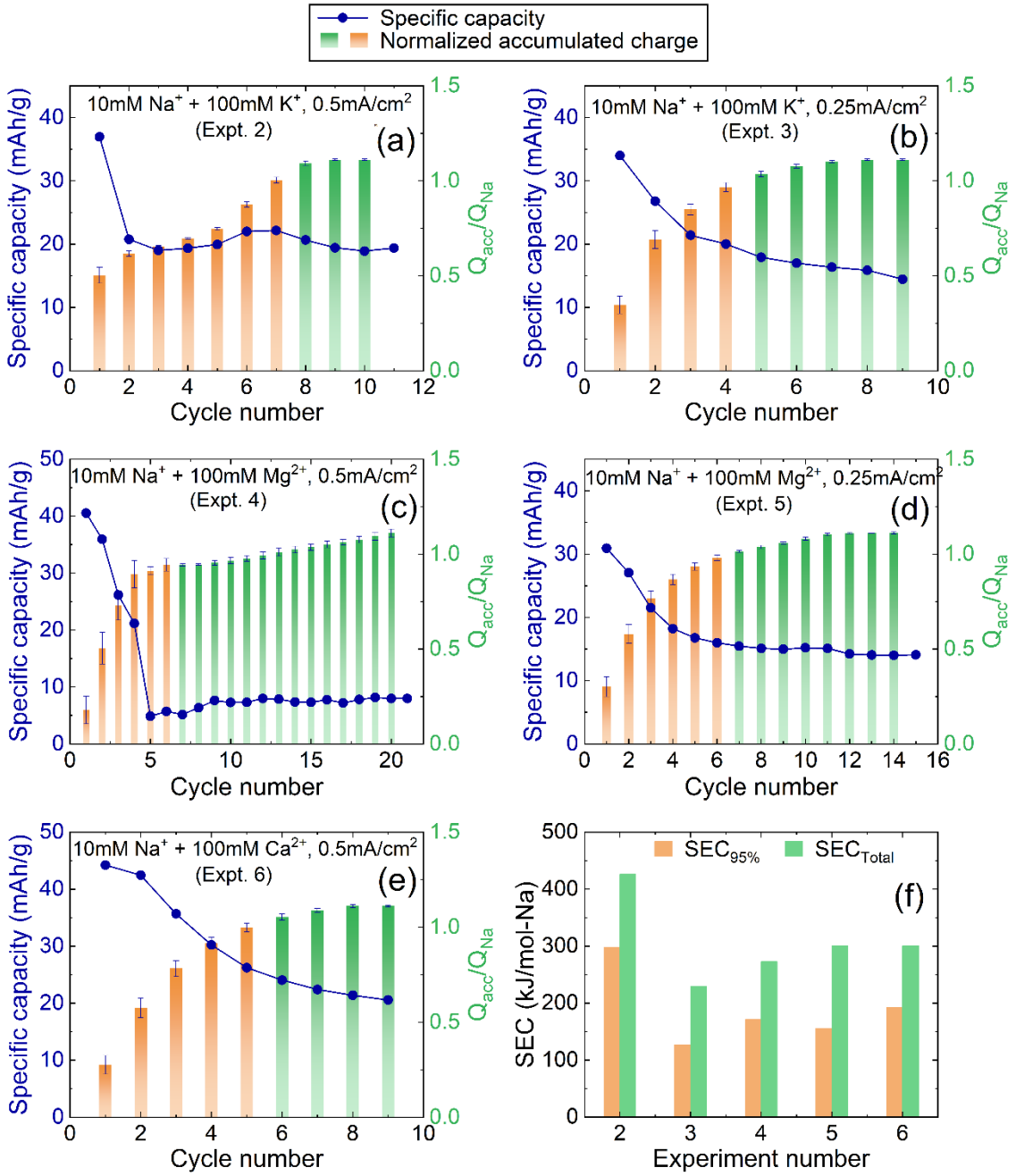

446

447 **Figure 6.** (a)-(e) Variation of specific capacity and normalized accumulated charge Q_{acc}/Q_{Na} with
448 cycle number during operation of an FDI cell using NTVP electrodes with feed solution and

applied current density as shown. Orange columns represent the cycles during which most Na^+ is removed, whereas green columns represent cycles that competing-ion adsorption is dominant (f) Total SEC compared to SEC calculated if the experiments were stopped after the cycle at which $Q_{acc}/Q_{Na} \geq 0.95$, as determined by the number of orange columns in the corresponding experiments: 4 cycles in Expt. 3; 5 cycles in Expt. 6; 6 cycles in Expts. 4 and 5; and 7 cycles in Expt. 2.

4. CONCLUSIONS

Sodium titanium vanadium phosphate powders coated with carbon (NTVP) were synthesized using a sol gel process and were shown to cycle stably in porous electrodes containing aqueous electrolytes with Na^+ and Li^+, reaching capacities of ~45 mAh/g for Na^+ intercalation and 30 mAh/g for Li^+ intercalation. NTVP showed no signs of intercalation for K^+, Mg^{2+}, and Ca^{2+} ions. These results indicate ultra-high selectivity of NTVP over other cations. The variation of potential with the degree of intercalation indicates an intercalation mechanism with limited miscibility gap for Na^+ that was shown to produce a phase-interaction energy of $0.57kT$ by fitting to a regular solution model. This interaction energy is larger than for Prussian blue analogues, but it is significantly lower than phase-separating NVP and NTP. Further, our theoretical modeling shows that the low phase-interaction energy of NTVP facilitates improved state-of-charge uniformity during the cycling of electrodes in FDI cells in which cation concentration gradients are inherent due to flow. In addition, experiments using a continuous-flow FDI apparatus containing NTVP electrodes were performed to determine the selectivity of Na^+ removal from solutions containing other cations, including K^+, Mg^{2+}, Ca^{2+}, Li^+ and NH_4^+. High process selectivity factors of 5 – 6 were obtained in cases with 1:10 Na^+:(K^+ or Mg^{2+}), with more than 90% removal of Na^+. Further, energy consumption less than 300 kJ/mol-Na was observed for all experiments, less than or

comparable to previous works which used a much lower concentration of competing cations. Therefore, symmetric FDI using NTVP electrodes is promising in terms of selective sodium removal when competing with other cations, which can have applications ranging from desalination for agricultural irrigation to the manufacture of high-purity chemicals. Future work involving optimization of electrodes and the FDI process can lead to significant reduction in overall energy consumption for sodium removal. Further, the reversible and selective intercalation of Li^+ in NTVP motivates its use for electrochemical lithium recovery, which to date has been limited to Li-ion battery materials (e.g., $LiFePO_4$[58]and $L_xM_2O_4$[59]).

ACKNOWLEDGMENTS

The US National Science Foundation (Award no. 1931659) and the Department of Mechanical Science and Engineering at the University of Illinois at Urbana-Champaign (UIUC) supported this research. X-ray diffraction and X-ray fluorescence experiments were performed at the Materials Research Laboratory at UIUC. We thank Nouryon Chemicals for providing Ketjen black material. We thank Dr. Erik Reale for assistance with initial experiments in the synthesis of NTVP and its testing in FDI.

SUPPORTING INFORMATION

Contents: X-ray diffraction results for NTVP, flooded-cell cycling results for NVP, potential curves for FDI cycling, FDI selectivity data table, IC measurement details, derivation of the regular solution potential model, and derivation of the theoretical model coupling SOC gradients to concentration gradients during FDI operation.

REFERENCES

1. Mekonnen, M. M. & Hoekstra, A. Y. Four billion people facing severe water scarcity. *Sci. Adv.* **2,** e1500323 (2016).

2. Haddeland, I., Heinke, J., Biemans, H., Eisner, S., Flörke, M., Hanasaki, N., Konzmann, M., Ludwig, F., Masaki, Y., Schewe, J., Stacke, T., Tessler, Z. D., Wada, Y. & Wisser, D. Global water resources affected by human interventions and climate change. *Proc. Natl. Acad. Sci.* **111,** 3251–3256 (2014).

3. Shiklomanov, I. & Rodda, J. World Water Resources at the Beginning of the Twenty-First Century. in *International Hydrology Series* (Cambridge University Press, 2003).

4. Zhang, J. L., Flowers, T. J. & Wang, S. M. Mechanisms of sodium uptake by roots of higher plants. *Plant Soil* **326,** 45–60 (2010).

5. Qian, Z., Miedema, H., de Smet, L. C. P. M. & Sudhȍlter, E. J. R. Modelling the selective removal of sodium ions from greenhouse irrigation water using membrane technology. *Chem. Eng. Res. Des.* **134,** 154–161 (2018).

6. USDA. Soil and Water Resources Conservation Act. *United States Dep. Agric.* 112 (2011).

7. Hopmans, J. W., Qureshi, A. S., Kisekka, I., Munns, R., Grattan, S. R., Rengasamy, P., Ben-Gal, A., Assouline, S., Javaux, M., Minhas, P. S., Raats, P. A. C., Skaggs, T. H., Wang, G., De Jong van Lier, Q., Jiao, H., Lavado, R. S., Lazarovitch, N., Li, B. & Taleisnik, E. Critical knowledge gaps and research priorities in global soil salinity. *Adv. Agron.* **169,** 1–191 (2021).

8. Ahdab, Y. D. & Lienhard, J. H. Desalination of brackish groundwater to improve water quality and water supply. in *Global Groundwater* 559–575 (Elsevier, 2021). doi:10.1016/B978-0-12-818172-0.00041-4

9. Cha, Y., Park, S. S., Kim, K., Byeon, M. & Stow, C. A. Irrigation with desalinated water: A step toward increasing water saving and crop yields. *Water Resour. Res.* 5375–5377 (2014). doi:10.1002/2013WR014979.Reply

10. Yermiyahu, U., Tal, A., Ben-Gal, A. & Bar-Tal, A. Rethinking Desalinated Water Quality and Agriculture. *Science (80-.).* **318,** 920–921 (2007).

11. Jones, E., Qadir, M., van Vliet, M. T. H., Smakhtin, V. & Kang, S. mu. The state of desalination and brine production: A global outlook. *Sci. Total Environ.* **657,** 1343–1356 (2019).

12. Zhang, X., Han, X., Yan, X., Chen, X., Jin, Z. & Hu, X. Continuous synthesis of high purity KNO3 through electrodialysis metathesis. *Sep. Purif. Technol.* **222,** 85–91 (2019).

13. Yoon, H., Lee, J., Kim, S. & Yoon, J. Electrochemical sodium ion impurity removal system for producing high purity KCl. *Hydrometallurgy* **175,** 354–358 (2018).

14. Han, L., Karthikeyan, K. G., Anderson, M. A. & Gregory, K. B. Exploring the impact of pore size distribution on the performance of carbon electrodes for capacitive deionization. *J. Colloid Interface Sci.* **430,** 93–99 (2014).

15. Chia-Hung Hou & Huang, C.-Y. A comparative study of electrosorption selectivity of ions by activated carbon electrodes in capacitive deionization. *Desalination* **314,** (2013).

16. Singh, K., Qian, Z., Biesheuvel, P. M., Zuilhof, H., Porada, S. & de Smet, L. C. P. M. Nickel hexacyanoferrate electrodes for high mono/divalent ion-selectivity in capacitive deionization. *Desalination* **481,** 114346 (2020).

17. Porada, S., Shrivastava, A., Bukowska, P., Biesheuvel, P. M. & Smith, K. C. Nickel Hexacyanoferrate Electrodes for Continuous Cation Intercalation Desalination of Brackish Water. *Electrochim. Acta* **255,** 369–378 (2017).

18. Shrivastava, A., Liu, S. & Smith, K. C. Linking capacity loss and retention of nickel hexacyanoferrate to a two-site intercalation mechanism for aqueous Mg 2+ and Ca 2+ ions. *Phys. Chem. Chem. Phys.* **21,** 20177–20188 (2019).

19. Shanbhag, S., Bootwala, Y., Whitacre, J. F. & Mauter, M. S. Ion Transport and Competition Effects on NaTi2(PO4)3 and Na4Mn9O18 Selective Insertion Electrode Performance. *Langmuir* **33,** 12580–12591 (2017).

20. Anantharamulu, N., Koteswara Rao, K., Rambabu, G., Vijaya Kumar, B., Radha, V. & Vithal, M. A wide-ranging review on Nasicon type materials. *J. Mater. Sci.* **46,** 2821–2837 (2011).

21. Senthilkumar, S. T., Han, J., Park, J., Min Hwang, S., Jeon, D. & Kim, Y. Energy efficient Na-aqueous-catholyte redox flow battery. *Energy Storage Mater.* **12,** 324–330 (2018).

22. Jian, Z., Hu, Y. S., Ji, X. & Chen, W. NASICON-Structured Materials for Energy Storage. *Adv. Mater.* **29,** 1–16 (2017).

23. Wang, H., Zhang, H., Cheng, Y., Feng, K., Li, X. & Zhang, H. All-NASICON LVP-LTP aqueous lithium ion battery with excellent stability and low-temperature performance.

Electrochim. Acta **278,** 279–289 (2018).

24. Jiang, Y., Zeng, L., Wang, J., Li, W., Pan, F. & Yu, Y. A carbon coated NASICON structure material embedded in porous carbon enabling superior sodium storage performance: NaTi 2 (PO 4) 3 as an example . *Nanoscale* **7,** 14723–14729 (2015).

25. Saravanan, K., Mason, C. W., Rudola, A., Wong, K. H. & Balaya, P. The first report on excellent cycling stability and superior rate capability of Na3V2(PO4)3 for sodium ion batteries. *Adv. Energy Mater.* **3,** 444–450 (2013).

26. Zhang, X., Rui, X., Chen, D., Tan, H., Yang, D., Huang, S. & Yu, Y. Na 3 V 2 (PO 4) 3 : An advanced cathode for sodium-ion batteries. *Nanoscale* **11,** 2556–2576 (2019).

27. Zhao, H. B., Hu, C. J., Cheng, H. W., Fang, J. H., Xie, Y. P., Fang, W. Y., Doan, T. N. L., Hoang, T. K. A., Xu, J. Q. & Chen, P. Novel rechargeable M3V2(PO4)3//Zinc (M = Li, Na) hybrid aqueous batteries with excellent cycling performance. *Sci. Rep.* **6,** 1–10 (2016).

28. Whitacre, J. F., Shanbhag, S., Mohamed, A., Polonsky, A., Carlisle, K., Gulakowski, J., Wu, W., Smith, C., Cooney, L., Blackwood, D., Dandrea, J. C. & Truchot, C. A Polyionic, Large-Format Energy Storage Device Using an Aqueous Electrolyte and Thick-Format Composite NaTi2(PO4)3/Activated Carbon Negative Electrodes. *Energy Technol.* **3,** 20–31 (2015).

29. Pang, G., Nie, P., Yuan, C., Shen, L., Zhang, X., Li, H. & Zhang, C. Mesoporous NaTi 2 (PO 4) 3 /CMK-3 nanohybrid as anode for long-life Na-ion batteries. *J. Mater. Chem. A* **2,** 20659–20666 (2014).

30. Chen, S., Wu, C., Shen, L., Zhu, C., Huang, Y., Xi, K., Maier, J. & Yu, Y. Challenges and

Perspectives for NASICON-Type Electrode Materials for Advanced Sodium-Ion Batteries. *Adv. Mater.* **29,** 1–21 (2017).

31. Han, J., Zarrabeitia, M., Mariani, A., Jusys, Z., Hekmatfar, M., Zhang, H., Geiger, D., Kaiser, U., Behm, R. J., Varzi, A. & Passerini, S. Halide-free water-in-salt electrolytes for stable aqueous sodium-ion batteries. *Nano Energy* **77,** 105176 (2020).

32. Van Nghia, N., Jafian, S. & Hung, I. M. Synthesis and Electrochemical Performance of the Na3V2(PO4)3 Cathode for Sodium-Ion Batteries. *J. Electron. Mater.* **45,** 2582–2590 (2016).

33. Jian, Z., Yuan, C., Han, W., Lu, X., Gu, L., Xi, X., Hu, Y. S., Li, H., Chen, W., Chen, D., Ikuhara, Y. & Chen, L. Atomic structure and kinetics of NASICON NaxV 2(PO4)3 cathode for sodium-ion batteries. *Adv. Funct. Mater.* **24,** 4265–4272 (2014).

34. Zhu, C., Song, K., A. van Aken, P., Maier, J. & Yu, Y. Carbon-Coated Na3V2(PO4)3 Embedded in Porous Carbon Matrix: An Ultrafast Na-Storage Cathode with the Potential of Outperforming Li Cathodes. *Nano Lett.* **14,** 2175–2180 (2014).

35. Reale, E. R., Regenwetter, L., Agrawal, A., Dardón, B., Dicola, N., Sanagala, S. & Smith, K. C. Low porosity, high areal-capacity Prussian blue analogue electrodes enhance salt removal and thermodynamic efficiency in symmetric Faradaic deionization with automated fluid control. *Water Res. X* **13,** 100116 (2021).

36. Gu, Y., Xiao, F., Xu, K., Pan, X., Li, J., Xu, C. & Zhou, X. Outstanding electrochemical performance of sodium vanadium phosphate cathode co-modified by carbon-coating and titanium-doping for Na-ion batteries. *Ceram. Int.* **45,** 12570–12574 (2019).

37. Klinser, G., Zettl, R., Wilkening, M., Krenn, H., Hanzu, I. & Würschum, R. Redox processes in sodium vanadium phosphate cathodes-insights from: Operando magnetometry. *Phys. Chem. Chem. Phys.* **21,** 20151–20155 (2019).

38. Zhao, W., Guo, L., Ding, M., Huang, Y. & Yang, H. Y. Ultrahigh-Desalination-Capacity Dual-Ion Electrochemical Deionization Device Based on Na3V2(PO4)3@C–AgCl Electrodes. *ACS Appl. Mater. Interfaces* **10,** 40540–40548 (2018).

39. Mason, C. W. & Lange, F. Aqueous ion battery systems using sodium vanadium phosphate stabilized by titanium substitution. *ECS Electrochem. Lett.* **4,** A79–A82 (2015).

40. Smith, K. C. & Dmello, R. Na-Ion Desalination (NID) Enabled by Na-Blocking Membranes and Symmetric Na-Intercalation: Porous-Electrode Modeling. *J. Electrochem. Soc.* **163,** A530–A539 (2016).

41. Smith, K. C. Theoretical evaluation of electrochemical cell architectures using cation intercalation electrodes for desalination. *Electrochim. Acta* **230,** 333–341 (2017).

42. Liu, S. & Smith, K. C. Quantifying the trade-offs between energy consumption and salt removal rate in membrane-free cation intercalation desalination. *Electrochim. Acta* **271,** 652–665 (2018).

43. Reale, E. R., Shrivastava, A. & Smith, K. C. Effect of conductive additives on the transport properties of porous flow-through electrodes with insulative particles and their optimization for Faradaic deionization. *Water Res.* **165,** 114995 (2019).

44. Son, M., Pothanamkandath, V., Yang, W., Vrouwenvelder, J., Gorski, C. A. & Logan, B. E. Improving the Thermodynamic Energy Efficiency of Battery Electrode Deionization

Using Flow-Through Electrodes. *Environ. Sci. Technol.* (2020). doi:10.1021/acs.est.9b06843

45. Pothanamkandathil, V., Fortunato, J. & Gorski, C. A. Electrochemical Desalination Using Intercalating Electrode Materials: A Comparison of Energy Demands. *Environ. Sci. Technol.* **54,** 3653–3662 (2020).

46. Wang, D., Bie, X., Fu, Q., Dixon, D., Bramnik, N., Hu, Y. S., Fauth, F., Wei, Y., Ehrenberg, H., Chen, G. & Du, F. Sodium vanadium titanium phosphate electrode for symmetric sodium-ion batteries with high power and long lifespan. *Nat. Commun.* **8,** 1–7 (2017).

47. Wang, E., Chen, M., Liu, X., Liu, Y., Guo, H., Wu, Z., Xiang, W., Zhong, B., Guo, X., Chou, S. & Dou, S. X. Organic Cross-Linker Enabling a 3D Porous Skeleton–Supported Na3V2(PO4)3/Carbon Composite for High Power Sodium-Ion Battery Cathode. *Small Methods* **3,** 1–10 (2019).

48. Jiang, X., Zhang, T. & Lee, J. Y. Does size matter – What other factors are limiting the rate performance of Na3V2(PO4)3 cathode in sodium-ion batteries. *J. Power Sources* **372,** 91–98 (2017).

49. Li, Z., Young, D., Xiang, K., Carter, W. C. & Chiang, Y.-M. Towards High Power High Energy Aqueous Sodium-Ion Batteries: The NaTi 2 (PO 4) 3 /Na 0.44 MnO 2 System. *Adv. Energy Mater.* **3,** 290–294 (2013).

50. Shrivastava, A. & Smith, K. C. Electron Conduction in Nanoparticle Agglomerates Limits Apparent Na + Diffusion in Prussian Blue Analogue Porous Electrodes . *J. Electrochem. Soc.* **165,** A1777–A1787 (2018).

51. Meethong, N., Huang, H. Y. S., Carter, W. C. & Chiang, Y. M. Size-dependent lithium miscibility gap in nanoscale Li 1-xFePO4. *Electrochem. Solid-State Lett.* **10,** 134–138 (2007).

52. Stringfellow, G. B. The calculation of regular solution interaction parameters between elements from groups III, IV and V of the periodic table. *Mater. Res. Bull.* **6,** 371–379 (1971).

53. Zelič, K. & Katrašnik, T. Thermodynamically Consistent and Computationally Efficient 0D Lithium Intercalation Model of a Phase Separating Cathode Particle. *J. Electrochem. Soc.* **166,** A3242–A3249 (2019).

54. Liu, S. & Smith, K. C. Intercalated Cation Disorder in Prussian Blue Analogues: First-Principles and Grand Canonical Analyses. *J. Phys. Chem. C* **123,** 10191–10204 (2019).

55. Guo, X., Wang, Z., Deng, Z., Li, X., Wang, B., Chen, X. & Ong, S. P. Water Contributes to Higher Energy Density and Cycling Stability of Prussian Blue Analogue Cathodes for Aqueous Sodium-Ion Batteries. *Chem. Mater.* **31,** 5933–5942 (2019).

56. Wessells, C. D., Peddada, S. V., Huggins, R. A. & Cui, Y. Nickel hexacyanoferrate nanoparticle electrodes for aqueous sodium and potassium ion batteries. *Nano Lett.* **11,** 5421–5425 (2011).

57. Guyes, E. N., Shocron, A. N., Chen, Y., Diesendruck, C. E. & Suss, M. E. Long-lasting, monovalent-selective capacitive deionization electrodes. *npj Clean Water* **4,** (2021).

58. Liu, C., Li, Y., Lin, D., Hsu, P. C., Liu, B., Yan, G., Wu, T., Cui, Y. & Chu, S. Lithium Extraction from Seawater through Pulsed Electrochemical Intercalation. *Joule* **4,** 1459–

1469 (2020).

59. Joo, H., Kim, S., Kim, S., Choi, M., Kim, S. H. & Yoon, J. Pilot-scale demonstration of an electrochemical system for lithium recovery from the desalination concentrate. *Environ. Sci. Water Res. Technol.* **6,** 290–295 (2020).